Magnetism in monatomic metal wires

2003 J. Phys.: Condens. Matter 15 S2533

(http://iopscience.iop.org/0953-8984/15/34/305)

INSTITUTE OF PHYSICS PUBLISHING JOURNAL OF PHYSICS: CONDENSED MATTER

J. Phys.: Condens. Matter **15** (2003) S2533–S2546 PII: S0953-8984(03)62916-4

Magnetism in monatomic metal wires

P Gambardella

Institut de Physique des Nanostructures, Ecole Polytechnique Fédérale de Lausanne, CH-1015 Lausanne, Switzerland

E-mail: pietro.gambardella@epfl.ch

Received 30 April 2003
Published 15 August 2003
Online at stacks.iop.org/JPhysCM/15/S2533

Abstract

The first investigation of magnetism in one-dimensional (1D) monatomic chains of metal atoms is reported. High-density arrays (5×10^6 cm^{-1}) of parallel Co atomic wires have been grown using the vicinal Pt(997) surface as a template. Angle-resolved photoemission experiments evidence the presence of a 3d exchange-split band for the Co wires giving rise to enhanced localized spin magnetic moments. X-ray magnetic circular dichroism shows further that the orbital magnetic moment is about five times larger compared to that of bulk hcp Co as a result of the reduced atomic coordination of the 1D wires. Whereas statistical models forbid long-range ferromagnetic order in infinite 1D spin chains at any temperature greater than zero, we show that finite monatomic Co chains display both short- and long-range ferromagnetic order. The chains consist of thermally fluctuating segments of ferromagnetically coupled atoms which evolve into a ferromagnetic metastable long-range-ordered state below 15 K. Ferromagnetism in 1D is stabilized by unusually large magnetic anisotropy energy barriers (2 meV/atom) which arise from the reduced dimensionality of the wires and related large orbital magnetization.

(Some figures in this article are in colour only in the electronic version)

1. Introduction

Fundamental magnetic properties such as spontaneous magnetization, magnetocrystalline anisotropy, and magnitudes of the spin (S) and orbital (L) atomic magnetic moments depend inherently on the dimensionality of a given system [1–5]. According to statistical mechanics, the tendency to magnetic order reduces as thermal fluctuations become more disruptive with decreasing dimensionality. As a result, magnetism in two-dimensional (2D) ultrathin films is more sensitive to temperature effects compared to that in 3D systems [6]. Indeed, owing to the reduced number of neighbours contributing to the exchange interaction, rigorous results for the isotropic Heisenberg model rule out ferromagnetic, antiferromagnetic, as well as oscillatory

long-range order in 2D and 1D [7, 8]. However, in 2D the introduction of dipolar coupling or of an arbitrarily small anisotropy of spin–orbit origin is sufficient to establish long-range magnetic order [9], while in 1D the Ising model, i.e., the extreme anisotropic limit of the Heisenberg Hamiltonian, still predicts zero magnetization in the absence of an external field at $T > 0$. Such conclusions apply to an ideal 1D lattice of spin point vectors. Linear chains of real atoms, however, differ substantially from a spin lattice model in that they have finite length, and S (L) arise from 3D spin (charge) densities distributed across the unit cell. Magnetic order in 1D systems consisting of real atoms is therefore an unsettled issue.

A further topic of fundamental importance is how S, L, and the magnetic anisotropy energy per atom, E_a, of a 1D system change with respect to those of the corresponding bulk elements. It is known that the reduced atomic coordination in thin films [1, 10–12] and small particles [4, 13, 14] significantly alters such quantities. In 1D, depending on the substrate chosen as a support, even stronger changes in S, L, and E_a are expected [15–23]. Theoretical models [24, 25] show that the magnetocrystalline anisotropy is connected via L and the spin–orbit interaction to the atomic structure of a magnetic material. There is therefore the possibility of enhancing the magnetic anisotropy by artificially decreasing the symmetry and coordination of magnetic aggregates, as is the case for 1D atomic chains. Theoretical calculations [16, 18, 19] show that values of E_a of the order of 10^{-3}–10^{-2} eV/atom can be attained, a factor 10^3 larger compared to those for bulk ferromagnetic metals.

Most experimental investigations on 1D magnetic systems have concentrated on insulator crystals consisting of arrays of linear chains of exchange-coupled transition metal (TM) ions separated by non-magnetic atom spacers and characterized by weak interchain interactions [26, 27]. One example is tetramethyl ammonium manganese chloride, which typically exhibits antiferromagnetic coupling and 1D paramagnetic behaviour down to about $T = 1$ K [28]. More recently, thanks to progress in molecular beam epitaxy at atomically ordered surfaces, investigations have focused on pure metal nanowires, whose thickness and spatial separation can be independently controlled. The atomic steps of a non-magnetic vicinal surface are used as a deposition template for TM atoms, thus producing a large number of nanowires in a parallel process. A small cost is paid in terms of the finite-size distribution of the wires with respect to, e.g., atom manipulation by scanning probes [29], but the large wire density allows one to use spatially integrating techniques with magnetic sensitivity such as Kerr magnetometry and x-ray magnetic circular dichroism (XMCD). This approach was first explored by Elmers *et al* [30] in the study of Fe wires on vicinal W(110), which show in-plane anisotropy and a relaxation-free ferromagnetic phase transition due to dipole-induced coupling across adjacent stripes [31, 32]. Shen *et al* [33, 34] found a pronounced temperature- and time-dependent magnetic relaxation for Fe stripes on stepped Cu(111) with out-of-plane anisotropy, due to the formation of 1D Ising-coupled spin blocks. Fe and Co stripes on Pd(110) and Ru(0001), respectively, have also been studied [35, 36].

In this study, we present the first experimental investigation of the magnetism of 1D metal chains in the monatomic limit. In section 2, we present the self-assembly approach that allows one to grow uniform arrays of 1D wires on a Pt stepped surface. We address the magnetic properties of 1D Co chains by analysing their valence band photoemission spectra (section 3) and XMCD data (section 4).

2. Self-assembly of Co monatomic chains

In this section we address the nucleation and growth of metals on densely stepped substrates with the aim of creating arrays of 1D nanowires with precise morphological characteristics. Depending on the surface temperature, adatoms on vicinal surfaces self-assemble into chain-

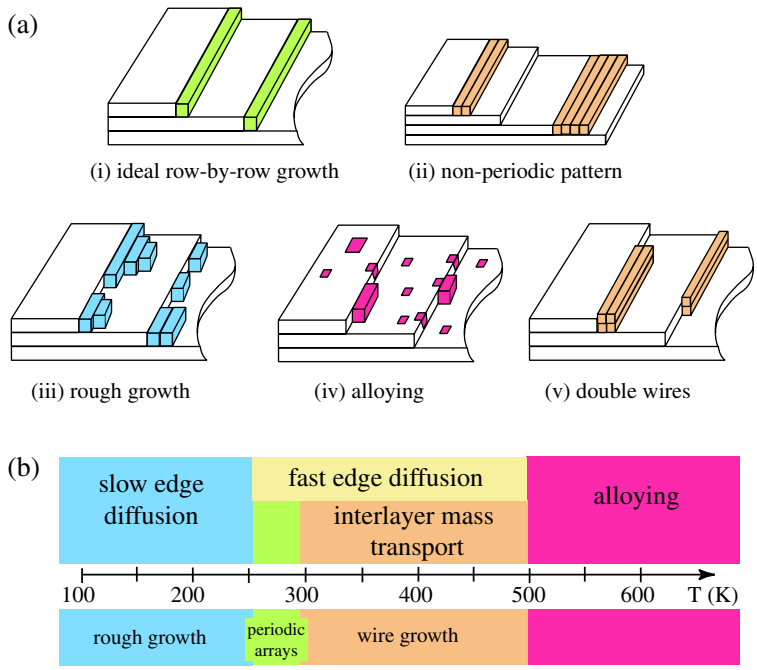

Figure 1. (a) Different growth modes on a stepped substrate. (b) Co growth modes on Pt(997) as a function of the substrate temperature. Although the temperature scale refers to the Co/Pt(997) system, this description applies to other metals such as Ag and Cu.

like structures by decorating the step edges. This is simply due to the increase of binding energy at the step sites [37, 38] and is, of course, a general phenomenon that holds for metals [39–44] as well as for gas species [45, 46]. An advantage of this growth method is that by adjusting the adatom coverage and the average step spacing one can independently control the wire width and separation, respectively. Growth proceeds either as a smooth step-wetting process [40–43] or as nucleation of two-dimensional (2D) islands at the step edges [47], provided that the adatom deplacement prior to nucleation is larger than the terrace width of the substrate. In figure 1 we show different scenarios of heteroepitaxy on a stepped substrate. We distinguish (i) the ideal case of row-by-row growth, (ii) wires of different widths due to interlayer crossing of the adatoms, (iii) formation of irregular 2D islands at the step edges, (iv) alloying, (v) formation of double-layer wires. In preparing arrays of 1D wires for photoemission and magnetic dichroism experiments, we have focused on the conditions that favour the ideal case (i). As a general trend we find that wire formation is limited at low temperature by slow edge-diffusion processes and at high temperature by interlayer diffusion and, eventually, by alloying between the metal adspecies and the substrate.

The basic requirement for growing self-assembled patterns of regular wires by step decoration is a good template. By this we mean a sample whose steps are as straight and as evenly spaced as possible. We have chosen to work with Pt vicinal surfaces since repulsive interactions between adjacent steps suppress step meandering [48], resulting in remarkably straight steps and in a narrow terrace width distribution, as shown in the scanning tunnelling microscopy (STM) image in figure 2(a). The average step separation as well as the kink density along the steps are determined by the crystal miscut. In the Pt(997) case, the average terrace width is 20.2 Å (figure 2(b)) with standard deviation $\sigma = 2.9$ Å [49], which allows one to obtain a density of 5×10^6 atomic wires cm^{-1}.

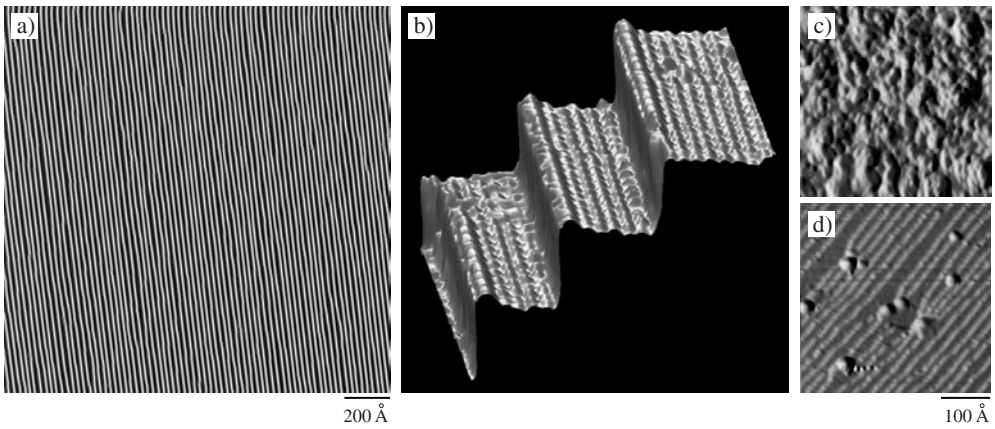

Figure 2. STM topographs of the Pt(997) surface. (a) Periodic step structure (each white line represents a monatomic Pt step). The step-down direction is from right to left. (b) A 3D close-up of the Pt steps (the vertical scale has been enhanced for better rendering). (c) Pt(997) after 10 min of sputtering at 300 K with a 800 eV Ar^+ beam at normal incidence. (d) Pt(997) after annealing in the presence of contaminants.

The cleaning of the sample is important for obtaining a regular periodic substrate. After sputtering at 300 K with a 800 eV Ar^+ beam, the stepped structure of the surface is completely lost (figure 2(c)). It can be recovered by annealing the surface at high temperature. To avoid uneven removal of material from the surface, however, the sample temperature is usually kept at $T = 750$ K during sputtering to allow sufficient mobility of the Pt atoms, and the ion beam is directed either normal to the surface or parallel to the steps. After repeated cycles of 800 eV Ar^+ sputtering at 750 K, the surface is annealed to 850 K, followed by a brief exposure to 1×10^{-7} mbar oxygen and by a flash to $T > 1000$ K to remove residual contaminant. Care has to be taken in cooling the sample at a slow enough rate (<40 K min^{-1}) down to 500 K in order to allow equilibration of the step morphology. Annealing in the presence of impurities might result in step pinning during the cool down of the surface (figure 2(d)).

Single Co atoms on Pt(111) terraces are mobile above $T = 55$ K. At higher temperature, as the terrace width of Pt(997) is small compared to the mean free path of Co adatoms, nucleation at the step sites occurs. The wire growth proceeds via incorporation of adatoms in 1D stable nuclei attached to the step edges [42]. However, below 250 K the wire formation is kinetically hindered by slow edge- and corner-diffusion processes. Regular Co wires grow only above 250 K [43], as shown in figure 3. A monatomic chain array is obtained as the coverage equals the inverse of the number of atomic rows in the substrate terraces, i.e., 0.13 monolayer (ML) (1 ML $= 1.5 \times 10^{-15}$ atoms cm^{-2}) for Pt(997). The average length of a continuous Co chain is estimated to be about 80 atoms from the average kink density per Pt step. As the coverage increases to more than a single monatomic wire per terrace, Co grows row by row (figures 4(a), (b)) up to $T = 290$ K. At $T > 290$ K, interlayer diffusion, i.e., the diffusion of adatoms across adjacent terraces, sets in. This implies that the proportionality between adlayer coverage on each terrace and terrace width is no longer valid, resulting in either or both (ii) and (v), shown in figure 1(a). As Co adatoms acquire enough thermal energy to cross the Pt–Co boundary at steps, bilayer Co wires and step bunching are observed (figure 4(c)).

Below 1 ML, the Co wires are pseudomorphic with the Pt substrate, implying that the Co lattice parameter is expanded by about 10% with respect to that of bulk hcp Co. In contrast to the case for deposition of Co on Pt(111) [50, 51], we do not observe a reconstruction of the

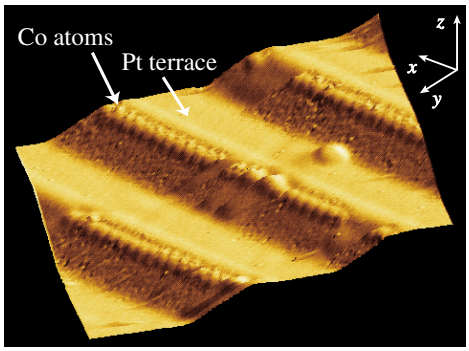

Figure 3. Co monatomic chains decorate the Pt step edges following deposition of 0.07 ML Co at $T = 250$ K (the vertical scale has been enhanced for better rendering). The chains are linearly aligned and have a spacing equal to the terrace width. The protrusion on the terrace is attributed to Co atoms incorporated in the Pt layer (from [67]).

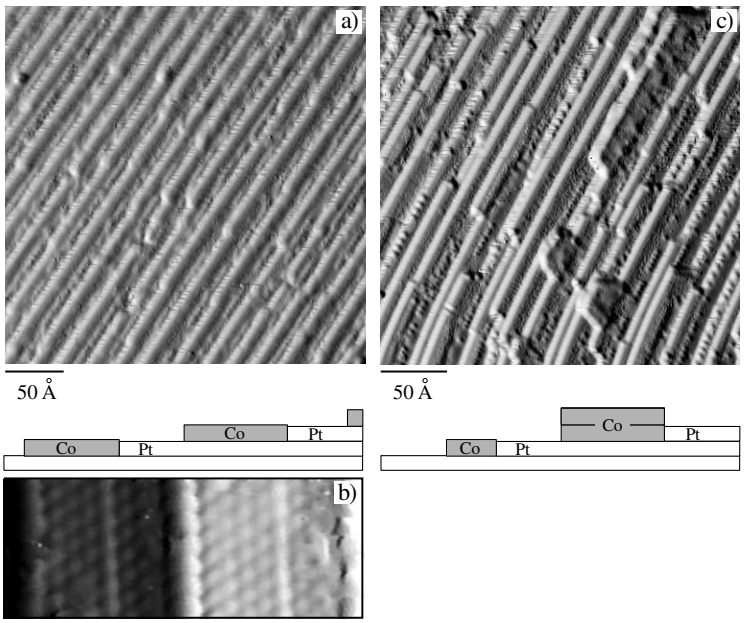

Figure 4. An STM image of 0.6 ML Co deposited at $T = 250$ K; the step-down direction is from right to left. Row-by-row growth conserves the original step pattern, forming regular stripes that run parallel to the Pt steps. (b) Detail of two adjacent terraces, as shown in the diagram, with atomic resolution on the Co chains and Pt substrate. (c) An STM image of 0.6 ML Co deposited at $T = 385$ K; the step-down direction is as in (a). Formation of bilayer Co wires with a non-periodic pattern.

substrate and the formation of dendrite-like islands, although stacking faults appear already at 250 K at the completion of the first Co overlayer [43]. At $T > 500$ K, significant Co–Pt alloying takes place. The temperature window for the growth of a regular periodic array of Co atomic chains is therefore limited to a narrow interval between 250 and 300 K, as edge diffusion is fast enough to have row-by-row growth and interlayer diffusion and intermixing are still inhibited (figure 1(b)).

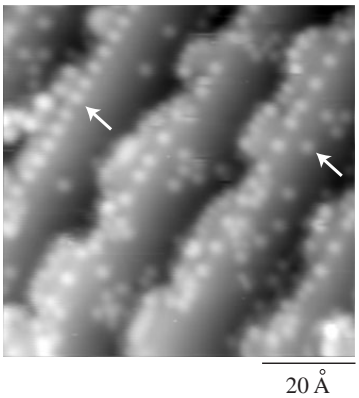

Figure 5. An STM image of 0.2 ML Ni deposited on Pt(997) at 200 K. The arrows indicate Ni atoms that have exchanged with Pt at step and terrace sites. The step-down direction is from right to left.

Not all combinations of substrate and overlayer are viable for inducing the self-assembly of monatomic chains. Ni, in contrast to Co, Ag, and Cu [42], is already diffusing into the Pt topmost layer at 150 K [44]. The adislands at this temperature have a rough 2D character; it is therefore impossible to find a temperature range where adatom diffusion is fast enough to lead to row-by-row growth prior to alloying. In the STM images, Ni atoms are imaged as bright protrusions (figure 5) along the step edges and on the terraces. Intermixing proceeds mainly via the substrate steps. Pt atoms that have exchanged with Ni are incorporated into the islands that decorate the step edges. A 2×1 Ni superstructure with 5.5 Å periodicity, i.e., two Pt lattice constants, forms confined to the step edges. This phase can be considered the 1D analogue of the $NiPt_3$ bulk alloy, where Ni atoms have only Pt nearest neighbours. The magnetic properties of such a 1D alloy have not been investigated here.

3. Electronic states of monatomic Co and Cu chains

The physical realization of 1D atomic systems opens up the possibility of investigating their magnetic behaviour and related electronic structure. Angle-resolved photoemission experiments have been performed at BESSY I in Berlin, at the TGM 5 undulator beamline. Considering the small coverage of Co that corresponds to a monatomic chain array on Pt(997), a serious problem encountered in the experiment was the isolation of the Co chain-induced states from the Pt 5d background in angle-resolved photoemission spectra. In order to increase the sensitivity to Co over Pt, we have exploited the difference in photon energy dependence of the 3d and 5d photoionization cross-sections. At a photon energy $h\nu = 40$ eV the spectra of clean Pt(997) and of the Co monatomic chains (0.12 ML Co) are nearly the same (figure 6(a), top). The presence of the Cooper minimum [52] in the Pt 5d cross-section at $h\nu = 150$ eV, however, significantly reduces the contribution of the Pt states for $h\nu > 100$ eV, so states with prevalent 3d character can be identified in the photoemission spectra (figure 6(a), bottom).

Figure 6(b) shows the evolution of the Co 3d states with Co coverage. Two features appear for the monatomic chains: one close to the Fermi level at about 0.3 eV and the other approximately at 2.4 eV binding energy. These features become more pronounced with increasing coverage, while their separation decreases. The observation of a double-peaked structure for the Co wires suggests the presence of a 1D exchange-split Co band [52].

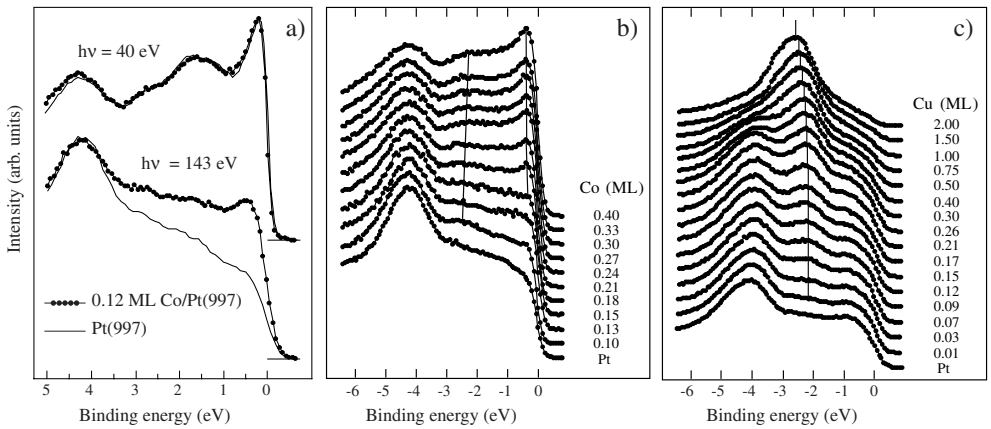

Figure 6. (a) Photoemission spectra of clean Pt(997) and after the deposition of 0.12 ML Co taken at a photon energy $h\nu = 40$ (top) and 143 eV (bottom). (b) Photoemission spectra of Co/Pt(997) taken at $h\nu = 122$ eV, 4° off normal emission, displaying the evolution of Co states with increasing Co coverage. The solid lines indicate the exchange-split Co 3d states. (c) Photoemission spectra of Cu/Pt(997) taken at $h\nu = 122$ eV at normal emission displaying the evolution of Cu states on Pt(997). A single peak is observed for the non-magnetic Cu d states (from [52]).

Exchange splitting is one key to magnetism since it creates a spin imbalance that produces a local magnetic moment. An approximate linear correlation between the 3d magnetic splitting and the local magnetic moment per atom has been found for TMs, where the 3d moment is of the order of 1 μ_B eV^{-1} times the exchange splitting [3]. For the Co monatomic chain-induced states, the exchange splitting is large (≈2.1 eV) compared to typical values for Co thin films (1.4–1.9 eV) and bulk Co (≈1.4 eV) [53–55]. This suggests in turn that S is considerably enhanced in the Co monatomic chains, of the order of 2.1 μ_B, in agreement with calculations [15, 17–19, 56]. Due to the 3d band broadening, the magnitude of the exchange splitting reduces with increased Co atomic coordination, as seen in figure 6(b) for coverages larger than 0.13 ML. In contrast to the case for Co, Cu chains on Pt(997) do not show evidence of local magnetic moments, presenting a single 3d feature at 2.3 eV binding energy. No Cu-induced states can be found close to the Fermi level because the Cu 3d shell is filled and the photoemission cross-section for sp states is very small in this photon energy range. The Cu 3d peak shifts to a higher binding energy above 0.17 ML and reaches 2.7 eV at 2.0 ML. The evolution of the Cu 3d state on Pt(997) also reflects changes in the electronic structure due to changes in the dimensionality of the system. The observed shift starts around 0.17 ML, in correspondence with the transition from a 1D to a 2D wire structure. For Cu on Pt(111), where large 2D island growth occurs, the Cu 3d peak is already found at 2.6 eV for coverages lower than 0.1 ML, as the atomic coordination already approaches that of a 2D ML [57].

4. Magnetism of Co monatomic chains

The valence band photoemission spectra presented in section 3 suggest the presence of enhanced S localized on the Co atoms in 1D chains. The magnetic behaviour of 1D wires has been further studied by XMCD, i.e., the absorption of circularly polarized x-rays in the soft-x-ray energy range (2p → 3d transitions) [58, 59]. XMCD is defined as a difference in absorption coefficients for parallel and antiparallel orientation of the helicity of the incident light with respect to the magnetization direction of the sample (figure 7). Because of its element

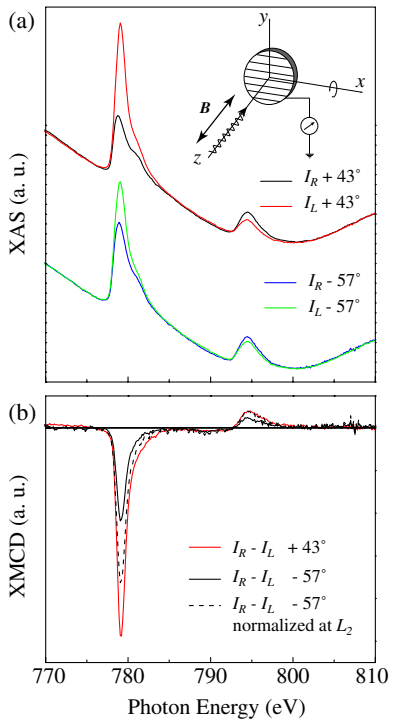

Figure 7. (a) Co monatomic chain x-ray absorption spectra for parallel (μ_+) and antiparallel (μ_-) directions of light polarization and field-induced magnetization ($T = 45$ K and $B = 6$ T). The μ_+-, μ_--spectra are taken with the field applied in the plane perpendicular to the chains at +43° off the (111) terrace normal in the step-up direction (top spectra, black and red (grey) solid curves, respectively) and −57° (bottom spectra, blue (dark grey) and green (light grey) solid curves, respectively). (b) The corresponding dichroic signal ($\mu_+ - \mu_-$) at +43° (red (grey) solid curve) and −57° (black solid curve). The dashed curve represents the XMCD at −57° normalized to the L_2 peak intensity at +43°.

selectivity and surface sensitivity (down to 3×10^{12} atoms cm^{-2} [4]), XMCD represents one of the most powerful magnetic probes available to date. The technique allows one to identify the magnetization direction and strength and to separately determine S and L for a given element by means of dipole sum rules [60–62]. The XMCD measurements were performed at beamline ID12B of the European Synchrotron Radiation Facility (ESRF) in Grenoble, where samples were prepared *in situ* at $T = 260$ K according to the procedure described in section 2. The Co coverage was controlled by cross-checking the coercive field of Co ultrathin films with those obtained at the EPF Lausanne in *in situ* Kerr–STM experiments. This method is consistent with the yield of a quartz microbalance and is extremely precise since the coercive field of Co on Pt depends critically on the Co coverage [63]. The absorption spectra were taken in the electron yield mode by measuring the drain current of the photoexposed sample for parallel and antiparallel alignment of the applied magnetic field $\boldsymbol{B}$ with the light helicity. All spectra have been normalized by the photocurrent emitted by a gold mesh positioned before the sample, which serves as a measure of the incident photon flux. The sample was rotated about its polar and azimuthal axes with respect to the incident light direction in order to measure the XMCD along different crystal orientations, as shown in the inset of figure 7.

Representative results for the XMCD at the Co $L_{2,3}$ absorption edges for the monatomic wires are shown in figure 7. The amplitude of the dichroic signal is a measure of the

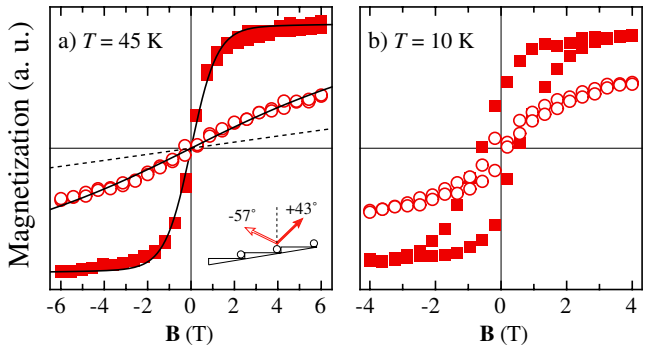

Figure 8. Magnetization of a monatomic wire array as a function of the applied field $\boldsymbol{B}$. The data points represent the Co L_3 XMCD at 779 eV normalized by the pre-edge intensity at 775 eV in order to eliminate the dependence of the electron yield on the sample orientation and magnetic field. (a) Magnetization at $T = 45$ K, in the easy direction (solid squares, +43°) and 80° away from the easy direction (empty circles, −57°) in the plane perpendicular to the wire axis (see the inset). The difference between the normalized L_3 XMCD at +43° and −57° at $\boldsymbol{B} = 6$ T corresponds to that of the XMCD spectra in figure 7. The solid curves are fits to the data. The dashed curve represents the magnetization expected for an isolated Co atom on Pt(997). (b) Magnetization at $T = 10$ K for the same geometry as in (a). Hysteretic behaviour sets in due to long-range ferromagnetic order. The unsaturated zero-field magnetization is attributed to the inhomogeneous lengths of the chains (from [67]).

magnetization of the Co wire array and contains information on the local character of the atomic moments. Due to the low Co coverage, the absorption edges of the monatomic wires are superimposed on a strong background originating from the oscillations following the Pt $N_{2,3}$ thresholds. The absorption by the non-magnetic substrate, however, does not contribute to the dichroic effect, as shown by the flat baseline of the Co XMCD in figure 7(b). The wires are characterized by a strong, angle-dependent dichroism that results from the alignment of the Co magnetic moments at $\boldsymbol{B} = 6$ T, $T = 45$ K. The easy magnetization direction of the monatomic chains lies in the plane perpendicular to the chain axis, tilted by +43° with respect to the (111) surface normal, where the positive sign indicates the step-up direction. The absorption spectra in figure 7(a) taken with the field applied parallel to the easy axis reveal a dichroic signal which is more than twice that obtained for the −57° direction. In the latter case, the applied 6 T field is not able to saturate the magnetization, thus indicating the presence of strong magnetic anisotropy, as discussed later.

The reduced atomic coordination of the monatomic chains compared to the bulk and 2D films has remarkable consequences for the magnitude of S and L. Calculations within the local spin density approximation (LSDA) scheme for Co/Pt(997) show that the narrowing of the Co 3d band and the corresponding increase in the density of states (DOS) at the Fermi level (E_F) increment S from the 1.57 μ_B/atom bulk value to 2.03 and 2.08 μ_B/atom for a ML and a 1D chain, respectively [56]; see also [17–19]. A larger relative increase is expected for L, which is generally more sensitive to changes in the atomic coordination [4]. Using the XMCD orbital sum rule [60], L can be experimentally determined from the integrated XMCD, $\int_{L_3+L_2}(\mu_+ + \mu_-)\,\mathrm{d}\varepsilon = \frac{C}{2\,\mu_B}L$, where ε is the photon energy and C is an experimental constant derived from the known bulk value $L = 0.15$ μ_B/atom and the bulk integrated XMCD [11]. For the monatomic wires we find $L = 0.68 \pm 0.05$ μ_B/atom, i.e., an enhancement of about a factor 5 compared to hcp Co. The monatomic chain L is significantly larger compared to that for 2D multilayers [10, 11, 64, 65], and also to that for 1 ML Co/Pt(111) ($L = 0.29$ μ_B/atom). In the 1D chains, the reduced coordination leads to a weaker hybridization of the Co states

and, consequently, to the enhancement of the local minority DOS at E_F, which leads to an increase in L [24, 25, 66]. Owing to the Co coordination dependence, larger values of L are found only in isolated Co adatoms and clusters with up to three atoms [4, 5].

In figure 8(a) we report the magnetic response of a set of monatomic wires at $T = 45$ K. The zero remanent magnetization reveals the absence of long-range ferromagnetic order. However, the shape of the magnetization curve indicates the presence of short-range order, i.e., of significant interatomic exchange coupling in the chains. For non-interacting paramagnetic moments, the magnetization expected in the present experimental conditions would be significantly smaller, as indicated by the dotted line in figure 8(a). The observed behaviour is that of a 1D superparamagnetic system, i.e., a system composed by segments, or spin blocks, each containing N exchange-coupled Co atoms, whose resultant magnetization orientation is not stable due to thermal fluctuations. A noticeable dependence of the magnetization on the direction of the applied field can be observed in figure 8. The strongest magnetic response is found in the +43° direction, as expected from the XMCD spectra in figure 7. Clearly, the shape of the superparamagnetic curves depends on the magnetic anisotropy energy of each spin block NE_a, as well as on N times the magnetic moment per Co atom. By fitting the curves in figure 8(a) assuming dominant uniaxial anisotropy and a classical model of the magnetization [67], we obtain $N = 15 \pm 1$ and $E_a = 2.0 \pm 0.2$ meV/atom. Thus, on average, about 15 Co atoms are coupled in each spin block at $T = 45$ K. A simple argument due to Landau [68] shows that this result does not contradict the spin lattice models treating magnetic order in 1D. Consider a chain consisting of N moments described by the Ising Hamiltonian $H = -J \sum_{i=1}^{N-1} S_{z\,i} S_{z\,i+1}$, with nearest-neighbour exchange coupling energy $J > 0$ (ferromagnetic interaction). The ground state energy of the system is $E_0 = -J(N-1)$ and corresponds to the situation where all the moments are aligned. The lowest-lying excitations are those in which a single break occurs at any one of the N sites, as shown below:

$\uparrow\uparrow\uparrow\uparrow\uparrow\uparrow\uparrow\uparrow\uparrow\uparrow\uparrow\uparrow\uparrow\uparrow\uparrow$ ground state,

$\uparrow\uparrow\uparrow\uparrow\uparrow\uparrow\uparrow\uparrow\uparrow\downarrow\downarrow\downarrow\downarrow\downarrow\downarrow$ lowest excited state.

There are $N-1$ such excited states, all with the same energy $E = E_0+2J$. At temperature T the change in free energy due to these excitations is $\Delta G = 2J - k_B T \ln(N-1)$. For $N \to \infty$ we have $\Delta G < 0$ at any finite temperature and the ferromagnetic state becomes unstable against thermal fluctuations. For $(N-1) < \mathrm{e}^{2J/k_B T}$, however, ferromagnetic order is energetically stable. Assuming $2J = 15$ meV [69, 70], we get an upper limit of $N = 50$ exchange-coupled atoms at $T = 45$ K. Measurements of the magnetization in the Co monatomic chains agree with this limit.

The large magnetic anisotropy energy of the monatomic chains (for comparison, $E_a = 45\ \mu$eV/atom in hcp Co [71]) is directly related [24, 25] to the anisotropy of L along the easy and hard directions. Although the XMCD sum rules cannot be applied far from saturation of the magnetization in the hard direction (−57°), the decrease of the L_3 XMCD intensity relative to L_2 (dashed curve in figure 7 (b)) indicates a significant orbital moment anisotropy [5], with $L(+43°) - L(-57°) \approx 0.12\ \mu_B$/atom. As expected, the spin–orbit coupling between L and S favours the direction where L is larger as the easy magnetization axis. The large anisotropy energy plays a major role in stabilizing long-range ferromagnetic order in 1D, in particular in inhibiting the approach to the thermodynamic limit described above. As in bulk ferromagnetic systems, anisotropy energy barriers can effectively pin the magnetization along a fixed direction in space. By lowering the sample temperature below $T_B = 15 \pm 5$ K, we observe a transition to a long-range ferromagnetically ordered state with finite remanence (figure 8(b)). The threshold temperature is the so-called blocking temperature, where the magnetization of each spin block

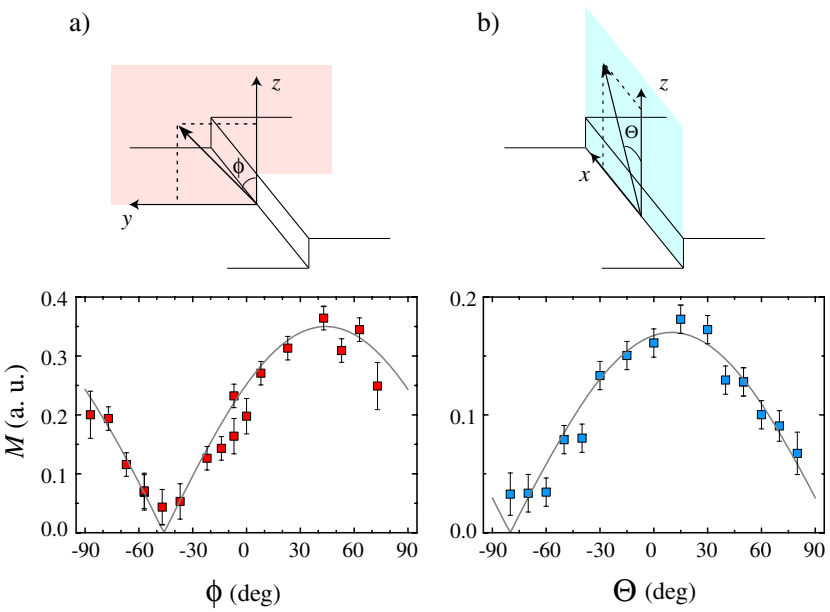

Figure 9. The angular dependence of the magnetization near remanence; (a) perpendicular, (b) parallel to the wire axis at 10 K. For each angle the magnetization has been aligned at $\boldsymbol{B} = 6$ T and subsequently measured near remanence at 0.25 T. A $|\cos(x - x_0)|$ dependence is found in both planes (solid curves), where $x = \Phi, \Theta$ (from [67]).

aligns along the common easy axis direction and the whole system becomes ferromagnetic. Long-range order in 1D atomic chains therefore enters as a metastable state thanks to slow magnetic relaxation. According to the Néel–Brown model of magnetization reversal [72], the relaxation time of a single-domain magnetic particle is expressed by an Arrhenius law of the form $\tau = \tau_0 \exp(\frac{E_a}{kT})$, where τ_0 is a prefactor of the order of 10^{-9} s. The anisotropy energy determined for a spin block, $NE_a = 31$ meV, is thus consistent with $T_B = 15$ K determined from the XMCD data, for which the timescale of the experimental observation requires $\tau \geqslant 10^2$ s.

As in 2D films, the magnetic anisotropy energy and the easy axis of magnetization are determined by the wire atomic structure and by the presence of the substrate. Tight-binding magnetic anisotropy energy calculations for free-standing and Pd-deposited Co monatomic chains [16] show that the easy direction rotates from parallel to perpendicular to the chain axis going from the free-standing to the Pd-supported chains. Here, the 1D geometry of the wires and the interaction with the stepped substrate are manifested by a strong uniaxial anisotropic behaviour and a tilted easy axis with respect to the sample in-plane and out-of-plane directions. Figure 9 shows the projection of the magnetization onto different directions with respect to the sample normal measured near remanence ($\boldsymbol{B} = 0.25$ T). As expected for a uniaxial system, the magnetization follows a $|\cos|$ function both in the plane perpendicular and that parallel to the wire axis, with a maximum in the perpendicular plane at +43°. Interactions of dipolar origin among adjacent chains are far too weak compared to the anisotropy energy of magnetocrystalline origin to influence the chain magnetization behaviour [16]. Further, we did not find evidence for interchain coupling effects mediated by the substrate [73], either of ferromagnetic or antiferromagnetic type, which would result in changes of T_B with respect to the value calculated by the Arrhenius law.

5. Conclusions

One-dimensional models have long been praised for their role in exemplifying and analysing many-body problems that are common to physics, chemistry, and statistics. It is only recently, however, that 1D systems made of real atoms have become the object of experiments. Arrays of parallel monatomic Co chains can be constructed on a Pt vicinal surface whose steps serve as a deposition template. A narrow temperature range exists where the Co chains grow row by row. Taking advantage of the uniformity and elevated density of the chain arrays, integral spectroscopic methods can be used to address the electronic and magnetic structure in 1D to 2D systems. The development of the Co wire-induced valence band states has been investigated by means of angle-resolved photoemission spectroscopy as a function of the wire thickness. We found a 3d exchange-split band for the Co chains which indicates the presence of enhanced spin magnetism in 1D. XMCD measurements provided the first experimental insights into the magnetic ordering phenomena of 1D atomic wires. Co monatomic chains sustain both short- and long-range ferromagnetic order depending on the substrate temperature. Owing to slow magnetic relaxation, ferromagnetic behaviour was observed in the monatomic chains without contradicting thermodynamic restrictions to long-range magnetic order in 1D. Ferromagnetism in 1D is stabilized by extraordinarily large magnetic anisotropy energy barriers which arise from large, unquenched orbital magnetic moments localized on the Co atoms and hybridization with the Pt substrate. Precise control of the atomic coordination in 1D systems represents a promising approach for understanding and tailoring magnetic anisotropy energy barriers in nanosized systems.

Acknowledgments

The author would like to acknowledge the people who have contributed to the measurements and to the discussion of the experimental results presented in this work: M Blanc, K Kuhnke, L Bürgi, O Jeandupeaux, H Brune, and K Kern (EPF Lausanne), C Carbone (Consiglio Nazionale delle Ricerche, Trieste, and Forschungszentrum Jülich), A Dallmeyer, K Maiti, M C Malagoli, W Eberhardt (Forschungszentrum Jülich), O Rader and C Pampuch (BESSY I), P Ohresser, S S Dhesi, N B Brookes, and K Larsson of beamline ID12B at the ESRF.

References

[1] Gradmann U 1993 *Handbook of Magnetic Materials* vol 7, ed K H J Buschow (Amsterdam: Elsevier) pp 1–96
[2] Schneider C M and Kirschner J 2000 *Handbook of Surface Science* vol 2, ed K Horn and M Scheffler (Amsterdam: Elsevier) pp 511–668
[3] Himpsel F J, Ortega J E, Mankey G J and Willis R F 1998 *Adv. Phys.* **47** 511 and references therein
[4] Gambardella P, Dhesi S, Gardonio S, Grazioli C, Ohresser P and Carbone C 2002 *Phys. Rev. Lett.* **88** 047202
[5] Gambardella P, Rusponi S, Veronese M, Dhesi S, Grazioli C, Dallmeyer A, Cabria I, Zeller R, Dederichs P, Kern K, Carbone C and Brune H 2003 *Science* **300** 1130
[6] Poulopoulos P and Baberschke K 1999 *J. Phys.: Condens. Matter* **11** 9495
[7] Mermin N D and Wagner H 1966 *Phys. Rev. Lett.* **17** 1133
[8] Bruno P 2001 *Phys. Rev. Lett.* **87** 137203
[9] Bander M and Mills D 1988 *Phys. Rev.* B **38** 12015
[10] Tischer M, Hjortstam O, Arvanitis D, Dunn J H, May F, Baberschke K, Trygg J and Wills J 1995 *Phys. Rev. Lett.* **75** 1602
[11] Weller D, Stöhr J, Nakajima R, Carl A, Samant M G, Chappert C, Mégy R, Beauvillain P, Veillet P and Held G 1995 *Phys. Rev. Lett.* **75** 3752
[12] Ohresser P, Ghiringhelli G, Tjernberg O and Brookes N 2000 *Phys. Rev.* B **62** 5803
[13] Billas I M L, Châtelain A and de Heer W A 1994 *Science* **265** 1682

[14] Dürr H A, Dhesi S S, Dudzik E, Knabben D, van der Laan G, Goedkoop J B and Hillebrecht F U 1999 *Phys. Rev.* B **59** R701
[15] Weinert M and Freeman A 1983 *J. Magn. Magn. Mater.* **38** 23
[16] Dorantes-Dávila J and Pastor G M 1998 *Phys. Rev. Lett.* **81** 208
[17] Komelj M, Ederer C, Davenport J and Fähnle M 2002 *Phys. Rev.* B **66** 140407(R)
[18] Lazarovits B, Szunyogh L and Weinberger P 2003 *Phys. Rev.* B **67** 024415
[19] Hong J and Wu R 2003 *Phys. Rev.* B **67** 020406(R)
[20] Eisenbach M, Györffy B, Stocks G and Újfalussy B 2002 *Phys. Rev.* B **65** 144424
[21] Spišák D and Hafner J 2002 *Phys. Rev.* B **65** 235405
[22] Bazhanov D, Hergert W, Stepanyuk V, Katsnelson A, Rennert P, Kokko K and Demangeat C 2000 *Phys. Rev.* B **62** 6415
[23] Bellini V, Papanikolaou N, Zeller R and Dederichs P 2001 *Phys. Rev.* B **64** 094403
[24] Bruno P 1989 *Phys. Rev.* B **39** 865
[25] van der Laan G 1998 *J. Phys.: Condens. Matter* **10** 3239
[26] Hone D and Richards P 1974 *Annu. Rev. Mater. Sci.* **4** 337
[27] Caneschi A, Gatteschi D, Lalioti N, Sangregorio C, Sessoli R, Venturi G, Vindigni A, Rettori A, Pini M and Novak M A 2001 *Angew. Chem. Int. Edn* **40** 1760
[28] Dingle R, Lines M and Holt S 1969 *Phys. Rev.* **187** 643
[29] Eigler D M and Schweizer E K 1990 *Nature* **344** 524
[30] Elmers H, Hauschild J, Höche H, Gradmann U, Bethge H, Heuer D and Köhler U 1994 *Phys. Rev. Lett.* **73** 898
[31] Hauschild J, Elmers H and Gradmann U 1998 *Phys. Rev.* B **57** R677
[32] Pietzsch O, Kubetzka A, Bode M and Wiesendanger R 2000 *Phys. Rev. Lett.* **84** 5212
[33] Shen J, Skomski R, Klaua M, Jenniches H, Manoharan S S and Kirschner J 1997 *Phys. Rev.* B **56** 2340
[34] Shen J, Klaua M, Ohresser P, Jenniches H, Barthel J, Mohan C and Kirschner J 1997 *Phys. Rev.* B **56** 11134
[35] Li D, Cuenya B R, Pearson J, Bader S and Keune W 2001 *Phys. Rev.* B **64** 144410
[36] Yu C, Li D, Pearson J and Bader S 2001 *Appl. Phys. Lett.* **79** 3848
[37] Gambardella P, Blanc M, Kuhnke K, Kern K, Picaud F, Ramseyer C, Girardet C, Barreteau C, Spanjaard D and Desjonquères M 2001 *Phys. Rev.* B **64** 45404
[38] Picaud F, Ramseyer C, Girardet C and Jensen P 2000 *Phys. Rev.* B **61** 16154
[39] Mundschau M, Bauer E and Swiech W 1989 *J. Appl. Phys.* **65** 581
[40] Himpsel F, Altmann K, Bennewitz R, Crain J, Kirakosian A, Lin J-L and McChesney J 2001 *J. Phys.: Condens. Matter* **13** 11097
[41] Himpsel F J and Ortega J E 1994 *Phys. Rev.* B **50** 4992
[42] Gambardella P, Blanc M, Brune H, Kuhnke K and Kern K 2000 *Phys. Rev.* B **61** 2254
[43] Gambardella P, Blanc M, Bürgi L, Kuhnke K and Kern K 2000 *Surf. Sci.* **449** 93
[44] Gambardella P and Kern K 2001 *Surf. Sci.* **475** L229
[45] Marsico V E, Blanc M, Kuhnke K and Kern K 1997 *Phys. Rev. Lett.* **78** 94
[46] Gambardella P, Šljivancanin Z, Hammer B, Blanc M, Kuhnke K and Kern K 2001 *Phys. Rev. Lett.* **87** 056103
[47] de la Figuera J, Huerta-Garnica M, Prieto J, Ocal C and Miranda R 1995 *Appl. Phys. Lett.* **66** 1006
[48] Papadia S, Desjonquères M and Spanjaard D 1996 *Phys. Rev.* B **51** 4083
[49] Hahn E, Schief H, Marsico V, Fricke A and Kern K 1994 *Phys. Rev. Lett.* **72** 3378
[50] Grütter P and Dürig U 1994 *Phys. Rev.* B **49** 2021
[51] Lundgren E, Stanka B, Koprolin W, Schmid M and Varga P 1999 *Surf. Sci.* **423** 357
[52] Dallmeyer A, Carbone C, Eberhardt W, Pampuch C, Rader O, Gudat W, Gambardella P and Kern K 2000 *Phys. Rev.* B **61** R5133
[53] Schneider C M, de Miguel J J, Bressler P, Schuster P, Miranda R and Kirschner J 1990 *J. Electron. Spectrosc. Relat. Phenom.* **51** 263
[54] Clemens W, Kachel T, Rader O, Vescovo E, Blügel S, Carbone C and Eberhardt W 1992 *Solid State Commun.* **81** 739
[55] Alkemper U, Carbone C, Vescovo E, Eberhardt W, Rader O and Gudat W 1994 *Phys. Rev.* B **50** 17496
[56] Bihlmayer G, Nie X and Blügel S 2001 private communication
[57] Shek M, Stefan P, Lindau I and Spicer W 1983 *Phys. Rev.* B **27** 7277
[58] Schütz G, Wagner W, Wilhelm W, Kienle P, Zeller R, Frahm R and Materlik G 1987 *Phys. Rev. Lett.* **58** 737
[59] Chen C T, Sette F, Ma Y and Modesti S 1990 *Phys. Rev.* B **42** 7262
[60] Thole B, Carra P, Sette F and van der Laan G 1992 *Phys. Rev. Lett.* **68** 1943
[61] Carra P, Thole B, Altarelli M and Wang X 1993 *Phys. Rev. Lett.* **70** 694
[62] Chen C T, Idzerda Y U, Lin H-J, Smith N V, Meigs G, Chaban E, Ho G H, Pellegrin E and Sette F 1995 *Phys. Rev. Lett.* **75** 152

[63] McGee N, Johnson M, de Vries J and aan de Stegge J 1993 *J. Appl. Phys.* **73** 3418
[64] Nakajima N, Koide T, Shidara T, Miyauchi H, Fukutan H, Fujimori A, Iio K, Katayama T, Nývlt M and Suzuki Y 1998 *Phys. Rev. Lett.* **81** 5229
[65] Anisimov A N, Farle M, Poulopoulos P, Platow W, Baberschke K, Isberg P, Wäppling R, Niklasson A M N and Eriksson O 1999 *Phys. Rev. Lett.* **82** 2390
[66] Ebert H, Zeller R, Drittler B and Dederichs P 1990 *J. Appl. Phys.* **67** 4576
[67] Gambardella P, Dallmeyer A, Maiti K, Malagoli M, Eberhardt W, Kern K and Carbone C 2002 *Nature* **416** 301
[68] Landau L and Lifshitz E 1959 *Statistical Physics* vol 5 (London: Pergamon)
[69] Pratzer M, Elmers H, Bode M, Pietzsch O, Kubetzka A and Wiesendanger R 2001 *Phys. Rev. Lett.* **87** 127201
[70] Frôta-Pessoa S and Kudrnovský R M J 2000 *Phys. Rev.* B **62** 5293
[71] Paige D, Szpunar B and Tanner B 1984 *J. Magn. Magn. Mater.* **44** 239
[72] Wernsdorfer W, Orozco E B, Hasselbach K, Benoit A, Barbara B, Demoncy N, Loiseau A, Pascard H and Mailly D 1997 *Phys. Rev. Lett.* **78** 1791
[73] Pratzer M and Elmers H 2002 *Phys. Rev.* B **67** 094416